NMPC-based Performance evaluation of Active Balancing Networks of Li-Ion Batteries for Overnight EV Charging

MUHAMMAD AZMAT ULLAH[1], AFAQ AHMED[1],ALI ARSHAD UPPAL[1],(SENIOR MEMBER, IEEE), AND QADEER AHMED[2], (SENIOR MEMBER, IEEE).

[1]Department of Electrical Engineering, COMSATS University Islamabad, Islamabad, Pakistan
[2]Mechanical and Aerospace Engineering, Scott Laboratory, 201 W 19th Ave, Columbus, OH 43210-1142

Corresponding author: Ali Arshad Uppal (e-mail: ali_arshad@comsats.edu.pk).

ABSTRACT A battery pack plays a vital role in an Electric Vehicle (EV), for it stores the energy and releases it to provide a reliable energy output. However, because of variations and imbalance in individual cell characteristics, the cells connected in a pack do not contain the same State of Charge (SoC) level—leading to poor EV performance and battery health deterioration. Therefore, in this work, active cell balancing is performed during overnight charging to ensure the same charge level among the cells by the end of the charging cycle. For this purpose, a high-fidelity mean current model is presented for a switched capacitor- (SC) based architecture comprising N cells for a generalized battery pack. Furthermore, this model is incorporated into a feedback control system utilizing Non-linear Model Predictive Control (NMPC). Since balancing losses are a primary factor during overnight charging, the SC-based NMPC is also compared with a buck-boost (BB) converter architecture under the same conditions. For each framework, extensive simulations are conducted by varying the weights of different terms in the cost function of the NMPC problem. The simulation results demonstrate that both SC- and BB-based architectures have been able to achieve balancing, wherein the average balancing time of SC is 186 % more than that of BB. However, in terms of average power losses and energy dissipation, SC incurred 288 % and 31 % fewer losses than BB, respectively.

INDEX TERMS Active cell balancing, bidirectional switched capacitor-based architecture, nonlinear model predictive control, overnight charging

I. INTRODUCTION

LITHIUM-ion batteries have become a prominent choice in the domain of energy-storage systems and particularly in Electric Vehicle (EVs) industries due to their high power and energy densities [1]. However, when a string of cells in a battery pack is connected in either series or parallel configuration, it is not naturally guaranteed that all the cells will assume the same charge level [2]. This disparity among charge levels largely originates from manufacturing inconsistencies and cell-to-cell variations and can have a drastic impact on the battery's health, performance, and energy utilization. To overcome these downsides, cell balancing is performed to ensure the even distribution of charge among all cells in a pack. Moreover, it can be categorized into two main types: passive and active cell balancing (ACB) [3]. The passive approach, though simpler to implement and control, is usually avoided as it tends to waste useful energy by

dissipating it through a resistor to make the cell with a higher charge equate with the one with a lower charge. ACB, on the other hand, can take on a much more complex structure and control scheme. However, this complexity comes with the flexibility of selecting different power electronic components–which act as intermediary storage devices to transfer charge among cells—charge transfer paths, control strategies, etc. This variation, along with hardware implementation, implies that each active cell balancing network (ACBN) is suited for a particular application, such as high-performance portable electronics or a grid-scale energy storage system, and subsequently yields different performance metrics, such as balancing time, balancing losses, energy efficiency, etc [4]. Moreover, various architectures that use different energy storage elements, such as capacitors and inductors or transformers, also face specific hardware and cost-related challenges. For instance, switched capacitor (SC)-

based architectures are cheaper and lighter than buck-boost (BB)-based ones, as the former utilizes the inductors, which are bulkier and more expensive than the simple ceramic or film capacitor. Subsequently, the costs associated with hardware implementation and scalability of BB are higher than those of SC-based architectures [5].

Similarly, in the context of EVs, a battery management system (BMS) performs cell balancing using various ACB variations to extend its range, remaining useful life, thermal management, etc. [6]–[8]. However, from a balancing perspective, an EV operates in three major modes: discharging, i.e., when the EV is operational on the road; charging, when the EV is connected to a charging station; and idle mode. Consequently, for each mode, a different ACB performance metric may be desirable. Therefore, in the following section, a thorough review of the different systems employed to perform balancing in different modes and their corresponding performance will be provided and evaluated.

A. LITERATURE REVIEW
The literature will start off with different variants of balancing architectures and their corresponding performances, and then it will shift focus to cases wherein the cell balancing is performed during the battery pack charging. For instance, [9] utilized a bi-directional multiple transformer flyback converter topology to perform active balancing. Since the objective was to re-utilize the used EV batteries, balancing was performed only at the start of the charge/discharge cycle to avoid the injection of current into the battery pack for a sustained duration. The simulation results reported a 13 % decrease in balancing losses and 8 % gain in discharge capacity compared to SoC-based and passive equalizations. Similarly, [10] also performed balancing in the context of reusable EV batteries. By employing a three-port Capacitor Inductor Capacitor Capacitor (CLCC) resonant converter and subsequently dividing the cell strings into two legs, the authors were able to reduce the number of bi-directional switches and gates to half as compared to conventional direct cell-to-cell topologies. Experiments were performed on 12 cells set up, and starting with an initial standard deviation of 243 mV, the equalizer was able to reduce it to 20 mV in 3400 s with a balancing efficiency of 96.3 %. Moreover, [11] used a single inductor-based circuit to perform both charge and voltage balancing for low-power applications such as wireless speakers and drones. Extensive simulations compared the performance metrics, such as power losses and balancing time, and using Pareto optimization, the authors attempted to find a balance between these metrics. Moreover, results, which were performed on 3 series-connected cells, showed the balancing was achieved in 2270 s with optimal balancing currents ranging from 0.65 A to 1.25 A. [12] combined the buck-boost converter (BB) and switched-capacitor-based techniques to perform balancing while simultaneously addressing the impact of parasitic resistances. By combining the two components using a switch array, which in turn was controlled by a complementary set of square waves, the framework eliminated the need for a high number of switches and a complex control structure. The experimental results performed on 10 cells revealed that the proposed system reduced the voltage difference from 132 to 18 mV in 55 minutes. Similarly, [13] integrated the BB and switched capacitors into a single system to perform cell balancing; the structure had the flexibility to transfer charge from any cell to another one in the pack while keeping the number of MOSFETs to a minimum. Performing the experiments on four and six series cells, the results demonstrated that, in comparison to conventional BB converter, the integrated structure achieved balancing three times faster and an efficiency increase of 17.3 %. [14] performed active cell balancing employing a transformer-based system in flyback configuration. This setup allowed for voltage monitoring and balancing at the same time by using a single transformer per cell, stressing the scalability, simplicity, and robustness of the proposed framework. Moreover, in experiments performed on a prototype comprising 16 parallel-connected cells, balancing was performed at the end of the charge cycle when any cell reached the threshold of 3.45 V, and subsequently balancing was achieved in about 0.75 hours. Similarly, ACB has also been involved in regulating and maintaining the temperature of a battery pack [15], [16], to increase the remaining useful life (RUL) [17], [18], and range enhancement of an EV [19], [20]. Focusing on balancing while charging, [21] performed cell balancing by employing a bi-directional DC-DC converter while also considering the balancing time during the charging phase. By considering the cell-to-pack-to-cell topology during charging, the system adopted the valley-filled equalization scheme, wherein the charge was transferred from the entire pack to the least charged cell. Experimental results demonstrated that a maximum 5 % of SoC difference was achieved during charging. Similarly, [22] also employed a dedicated DC/DC converter for each cell to perform cell balancing while also considering the variation in cells' parameters. The strategy involved the precise measurements of State of Health (SoH) and SoC, and the focus was on achieving fast charging while simultaneously minimizing SoCs differences and output voltage ripple. [23] proposed a three-stage strategy in which charging and subsequent balancing were performed. Each stage was distinguished by varying levels of charging and balancing currents, which were controlled by MSP430 microcontroller and logic-based switching. Experiments revealed that voltage difference of 0.05 V was achieved in about 3600 s. With the focus of increasing the pack's capacity and lowering computational BMS cost , [24] performed balancing based on charging cell voltage curves (CCVC); the strategy involved determining the amount of charge required by each cell based on their voltage profile during charging. Results demonstrated a 13.03% improvement in capacity upon balancing. Mainly focusing on improving equalization speed during charging, [25] employed a closed-loop switched-capacitor structure. The strategy involved determining the shortest path among cells to transfer charge. Simulation results revealed that a

maximum difference of 0.1 V and up to 95% efficiency are achieved all the while improving the balancing speed. [26] focused on developing strategies, each tailored for charging and discharging phases. An inductor was used as an energy-storage element, and both schemes fundamentally relied on measuring average SoC level. Moreover, the work also formulated the relation between balancing time and balancing architecture's parameters, such as capacity, inductance, switching frequency, etc. In the same vein, [27] also developed charging and discharging strategies while balancing. The systems worked in two steps: pack charging and individual cell charging, wherein the latter step was dedicated to cell balancing, and switching between these modes was decided on a certain voltage threshold value. Moreover, there also have been studies performing balancing while charging using passive techniques. For instance, to enable fast charging in passive cell balancing, [28] utilized variable resistors in parallel combination, wherein certain resistors were actively selected whilst charging to enable higher balancing currents, which reduced balancing time.

B. GAP ANALYSIS

In literature, different balancing systems that comprise various power electronics components have been investigated. However, most studies lack the manifestation of the advantages of ACB at a practical level, especially in the context of an EV. Furthermore, for an EV plugged into a charging station for an overnight charge, it is more desirable to reduce the balancing losses than the balancing time during cell balancing. From literature, it is obvious that for these metrics, the selection of electronic components plays an integral role. However, for these models—ACB circuits comprising various components—to yield accurate values of the performance metrics, incorporation of a high-fidelity model of balancing currents and power losses is integral, as demonstrated in our earlier study [29]. Building upon that, in [30], we derived a high-fidelity model for a BB balancing circuit comprising two cells and performed balancing using simple logic-based control. Subsequently, in [31], [32], we brought the same model under a non-linear model predictive control (NMPC) framework to perform cell balancing. Since it has been established from the literature that NMPC is the prime control technique for systems having input/output constraints, nonlinearities, and conflicting objectives—all these features are exhibited by ABCN. Therefore, keeping in mind the lack of investigation of ACB performance for overnight EV charging under high-fidelity modeling and optimal control framework, the major contributions of this work are given below.

MAJOR CONTRIBUTIONS

The major contributions of this work are as follows:
- Mathematical modeling of high-fidelity currents and power losses for a switched capacitor-based (SC) architecture for a generalized N-series connected lithium-ion cells.

- Formulation of an NMPC problem for generalized N-cells to actively distribute energy among cells while incorporating a trade-off between balancing time and power losses.
- Demonstration of efficacy of SC over BB-based architecture for overnight EV charging by conducting extensive simulation, comparative analysis, and evaluating performance metrics under NMPC-based framework

The rest of the paper is distributed as follows: in Section II high-fidelity balancing currents and power losses based SC architecture comprising N serially connected cells is modeled; moreover, in Section III, NMPC problem is formulated for the above generalized problem; similarly, Section IV provides a detailed discussion on the comparative performance of SC and BB-based architecture; and finally, the paper is concluded in Section IV.

II. MATHEMATICAL MODELING OF SWITCHED CAPACITOR BASED ACBN
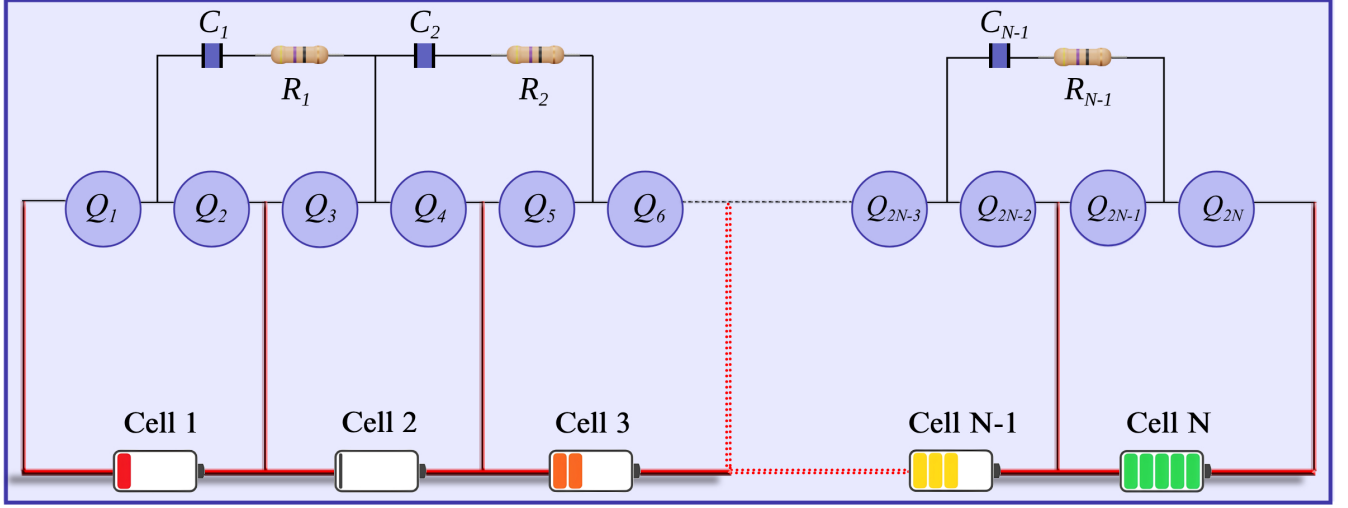
In the present study, an SC-based architecture is presented, which is shown in Figure 1. The battery pack consists of N number of series-connected Li-ion cells and is equipped with $N-1$ number of SC converters with $2N$ MOSFETs acting as switches. It can be seen from Figure 1 that for each switched capacitor C_i, where $i = (1, 2, \ldots, N-1)$, there are four switches $Q_{i,j}$ attached, where j represents the one pair of MOSFET attached to C_i such that $j \in S = \{1, 2\}$. To further dispel doubt about indexing notations, the working principle of the SC-based architecture is outlined next. Each switch pair $Q_{i,j}$ consists of two MOSFETs that always turn on and off simultaneously and $Q_{i,1}$ is used for the odd pair and $Q_{i,2}$ for the even pair of switches. During the charging cycle, when cell-1 is at a higher SoC than cell-2, the MOSFET pair $Q_{1,1}$ is turned on and cell-1 completes the path with the capacitor C_1 and transfers excess energy to it. During the discharging phase, the MOSFET pair $Q_{1,2}$ is turned on, and the charged C_1 transfers the energy to the adjacent lower SoC cell-2. Likewise, excess energy from the center sandwiched cells is transferred to both neighboring cells, while cells (cell-1 and cell-N) connected at the edges transfer excess energy to only one adjacent cell.

Furthermore, a simple equivalent circuit model (ECM) is taken to demonstrate the dynamic behavior of Li-ion battery cells in the battery pack, and a high-fidelity mathematical model of SC architecture, which is formulated using mean balancing currents and power losses of the SC, is adopted from [30] and is further extended to serially connected N-cells.

A. EQUIVALENT CIRCUIT MODEL OF BATTERY PACK

The control oriented mathematical model of our battery pack system representing SoC levels of N cells connected in series, is given by the following equations:

$$\dot{\mathbf{x}} = \mathbf{f}(\mathbf{x}, \mathbf{u}), \tag{1}$$

FIGURE 1: Switching capacitor based ACBN for N number of series connected cells

$$\mathbf{f}(\mathbf{x}, \mathbf{u}) = \begin{bmatrix} \dfrac{I_{b_1}(\mathbf{x}, \mathbf{u})}{\eta_1} & \dfrac{I_{b_2}(\mathbf{x}, \mathbf{u})}{\eta_2} & \cdots & \dfrac{I_{b_N}(\mathbf{x}, \mathbf{u})}{\eta_N} \end{bmatrix}^T \quad (2)$$

$$v_i = \sum_{j=1}^{8} p_j x_i^{(8-j)}, \quad (3)$$

where the state vector $\mathbf{x} = \begin{bmatrix} x_1 & x_2 & \cdots & x_N \end{bmatrix}^T$ is the SoCs of the cell and $\mathbf{f} : \mathbb{R}^N \times \mathbb{R}^{2(N-1)} \to \mathbb{R}^N$ is the nonlinear function of x and u, where $\mathbf{u} = \{u_{i,j}\}$ is the control input vector that represents duty cycles of MOSFETs; η_n denotes the cell capacity, measured in (Ah); I_{b_n} is the current (A) of the cell n, where $n = 1, 2, \cdots, N$; and v_n represents the open circuit voltage (OCV) of a cell, and $\mathbf{p} = [88.56, -320.46, 472.36, -368.96, 166.57, -44.01, 7.18, 2.95]$, which represents the relation between the cell's OCV and its SoC. The OCV–SOC data corresponds to Li-ion battery model LG 186550HG2 and was obtained from [33]. Subsequently, a 7th order polynomial was fitted on that data set to accurately capture and represent the cell's voltage characteristics.

The expression of the currents of the cells, as per position of the cells within the battery pack, are given as under:

$$I_{b_1} = \tilde{I}_{1,1}(x_1, u_{1,1}, v_{l_1}, v_{h_1}) + I_e,$$
$$\vdots$$
$$I_{b_{n \in [2, N-1]}} = \tilde{I}_{n-1,2}(x_{n-1}, x_n, u_{n-1,2}, v_{h_{n-1}}, v_{l_{n-1}})$$
$$+ \tilde{I}_{n,1}(x_n, x_{n+1}, u_{n,1}, v_{l_n}, v_{h_n}) + I_e,$$
$$\vdots$$
$$I_{b_N} = \tilde{I}_{N-1,2}(x_{N-1}, x_N, u_{N-1,2}, v_{h_{N-1}}, v_{l_{N-1}}) + I_e, \quad (4)$$

where $\tilde{I}$ is the charging and discharging current (also termed as balancing currents) of switching capacitor i; v_{h_i} and v_{l_i} are the high and low open-circuit voltages of the adjacent cells corresponding to the ith capacitor and I_e is the constant charging current provided to charge the cells.

B. MEAN BALANCING CURRENTS IN SC BASED ACBN

The high-fidelity model of mean balancing currents, which contains various dynamic and static parameters of ACBN, is adopted from [30] and is generalized for N cells. The mean current of the switching capacitor during one switching period is given as:

$$\tilde{I}_{i,j} = \frac{\Delta Q_i}{T} = \frac{C_i \Delta V_{i,j}}{T}, \quad (5)$$

where $\Delta V_{i,j}$ represents the voltage ripple, which denotes the fluctuation in the capacitor voltage due to inter cells charge transfer and is defined as follows:

$$\Delta V_{i,j} = (v_{l_i} - v_{h_i}) \tanh\left(\frac{u_{ij}T - t_d}{2\tau_i}\right)$$

$$\tilde{I}_{i,j} = \frac{C_i}{T}(v_{l_i} - v_{h_i}) \tanh\left(\frac{u_{ij}T - t_d}{2\tau_i}\right)$$

$$\tilde{I}_{i,j} = \frac{C_i}{T}(v_{l_i} - v_{h_i})(\Delta U_{i,j})$$

$$\Delta U_{i,j} = \frac{1 - e^{\frac{t_d - u_{i,j}T}{\tau_i}} - e^{\frac{u_{i,j}T - T + t_d}{\tau_i}} + e^{\frac{2t_d - T}{\tau_i}}}{1 - e^{\frac{2t_d - T}{\tau_i}}} \quad (6)$$

$$\tau_i = R_i C_i, \quad R_i = R_{c,i} + R_0 + 2 \cdot R_{ds_{on}}, \quad (7)$$

where the parameter t_d represents the dead time introduced to prevent short circuits; T is the switching period and is $= \frac{1}{f}$, with f being the switching frequency. The time constant of the circuit is $\tau_i = R_i C_i$, with R_i is the equivalent resistance of the charging and discharging path of the corresponding SC, and C_i is the capacitance of the balancing capacitor; R_{c_i} is the resistance of the ith capacitor; R_0 is the series resistance of the cell (also termed as internal resistance) and $R_{ds_{on}}$ is the resistance of the MOSFET during on time, respectively.

C. POWER LOSSES

The presented model accounts for various power losses in the ACBN and are mainly categorized as conduction losses and switching losses. The detailed description are given as follows:

CONDUCTION LOSSES

The conduction losses are those losses which occur due to internal resistances of the cell, parasitic resistances of the energy storing elements and on-state resistances of the MOSFETs, and are given by:

$$P_{\text{cond}} = \sum_{i=1}^{N-1} \sum_{j=1}^{2} \left[I_{c_{i,j}}^2 R_i u_{i,j} + I_{d_{i,j}}^2 R_i u_{i,j} \right], \quad (8)$$

$$I_{c_{i,j}} = \sqrt{ \frac{\tau_i \left(v_{h_i} - v_i \right)^2}{2\, T\, R_i^2} \left(1 - e^{2 \left(t_d - u_{ij} T \right)/\tau_i} \right)}, \quad (9)$$

$$I_{d_{i,j}} = \sqrt{ \frac{\tau \left(v_{l_i} - v_i \right)^2}{2\, T\, R_i^2} \left(e^{2 \left(u_{ij} T - T + t_d \right)/\tau_i} - 1 \right)}, \quad (10)$$

where $I_{c_{i,j}}$ and $I_{d_{i,j}}$ are the root-mean-square (RMS) charging and discharging currents of the ith capacitor, and v_i is its voltage during the duty cycle $u_{i,j}$.

RISE TIME LOSSES

Moreover, switching losses also consist of rise-time and fall-time losses, where rise-time losses are defined as:

$$P_{r_{i,\tilde{j}}} = \frac{1}{T} \left(\int_{0.2\, t_r}^{0.3\, t_r} \left[\left(\frac{(0.1\, v_{h_i} - v_{h_i})\, (t - 0.2\, t_r)}{0.1\, t_r} + v_{h_i} \right) \right. \right.$$
$$\left. \left. \times \left(\frac{(0.7\, I_{\max_{i,j}})\, (t - 0.2\, t_r)}{0.1\, t_r} \right) \right] dt \right) \quad (11)$$

$$P_{r_{i,\tilde{j}+2}} = \frac{1}{T} \left(\int_{0.2\, t_r}^{0.3\, t_r} \left[\left(\frac{(0.1\, v_{l_i} - v_{l_i})\, (t - 0.2\, t_r)}{0.1\, t_r} + v_{l_i} \right) \right. \right.$$
$$\left. \left. \times \left(\frac{(0.7\, I_{\max_{i,j}})\, (t - 0.2\, t_r)}{0.1\, t_r} \right) \right] dt \right) \quad (12)$$

where $\tilde{j}$ refers to the first MOSFET of $\forall\, j \in S$, similarly, $\tilde{j} + 2$ refers to the second MOSFET of $\forall\, j \in S$; $I_{\max_{i,j}}$ is the maximum current during the switching transition of the MOSFETS associated with ith capacitor; t_r is the switch rise time; and

$$I_{\max_{i,j}} = \frac{1}{R_i} (v_{h_i} - v_{l_i}) \frac{e^{(u_{ij} T - t_d)/\tau_i}}{1 + e^{(u_{ij} T - t_d)/\tau_i}}. \quad (13)$$

$$P_{r_i} = 2 P_{r_{i,\tilde{j}}} + 2 P_{r_{i,\tilde{j}+2}} \quad (14)$$

$$P_{r_{\text{total}}} = \sum_{i=1}^{N-1} P_{r_i}, \quad (15)$$

FALL TIME LOSSES

Similarly, the switching power losses during the fall time are given as:

$$P_{f_{i,\tilde{j}}} = \frac{1}{T} \left(\int_{0.2\, t_{fall}}^{0.3\, t_{fall}} \left[\left(\frac{(0.1\, v_{h_i} - v_{h_i})\, (t - 0.2\, t_{fall})}{0.1\, t_{fall}} + v_{h_i} \right) \right. \right.$$
$$\left. \left. \times \left(\frac{(0.7\, I_{\min_{i,j}})\, (t - 0.2\, t_{fall})}{0.1\, t_{fall}} \right) \right] dt \right) \quad (16)$$

$$P_{f_{i,\tilde{j}+2}} = \frac{1}{T} \left(\int_{0.2\, t_{fall}}^{0.3\, t_{fall}} \left[\left(\frac{(0.1\, v_{l_i} - v_{l_i})\, (t - 0.2\, t_{fall})}{0.1\, t_{fall}} + v_{l_i} \right) \right. \right.$$
$$\left. \left. \times \left(\frac{(0.7\, I_{\min_{i,j}})\, (t - 0.2\, t_{fall})}{0.1\, t_{fall}} \right) \right] dt \right), \quad (17)$$

where $I_{\min_{i,j}}$ is the minimum current during the switching transition of the MOSFETS associated with ith capacitor; t_{fall} is the switch fall time; and

$$I_{\min_{i,j}} = \frac{1}{R_i} (v_{h_i} - v_{l_i}) \frac{1}{1 + e^{(u_{ij} T - t_d)/\tau_i}} \quad (18)$$

$$P_{f_i} = 2 P_{f_{i,\tilde{j}}} + 2 P_{f_{i,\tilde{j}+2}} \quad (19)$$

$$P_{f_{\text{total}}} = \sum_{i=1}^{N-1} P_{f_i} \quad (20)$$

TOTAL SWITCHING AND OVERALL LOSSES

Consequently, the total switching losses are then the total summation of both the fall time and rise time losses; thus they are given as:

$$P_{total_{sw}} = P_{r_{\text{total}}} + P_{f_{\text{total}}}$$

Similarly, total power losses of the SC-based ACBN consist of conduction and switching power losses:

$$P_{\text{loss}} = P_{\text{cond}} + P_{total_{sw}}$$

III. NON LINEAR MODEL PREDICTIVE CONTROL OF ACTIVE CELL BALANCING

The NMPC problem is formulated, and subsequently solved, to achieve twofold agenda: cell balancing and reduced power losses. However, these two sub-objectives are conflicting in nature; therefore, they need to be assigned proper weights to reach a balance. Therefore, NMPC problem is formulated as follows:

$$\min_{\mathbf{x}(k),\mu(k)} J(\mathbf{x}(k), \mu(k)), \quad (21)$$

where

$$J = \sum_{k=k_0}^{k_0 + N_p} \left[w_x \sum_{n=1}^{N} \left\{ \tilde{x}_n(k)^2 \right\} + w_p P_{loss}(k) \right],$$

$$\tilde{x}_n(k) = x_n(k) - \frac{1}{N} \sum_{n=1}^{N} x_n(k).$$

subject to,

$$\mathbf{x}(k + 1) - f(\mathbf{x}(k), \mu(k)) = 0, \qquad (22a)$$

$$\mathbf{x}(k_0) = \mathbf{x}_{k_0}, \qquad (22b)$$

$$\mu(k) \in \mathcal{U}, \qquad (22c)$$

$$\mathbf{x}(k) \in \mathcal{X}. \qquad (22d)$$

The optimization problem is formulated over a prediction horizon N_p. Moreover, $w_x, w_p \in \mathbb{R}^+$ are the scalar weights coefficients which represent the trade-off between SoC balancing and power losses, and determine the relative importance of minimizing the charge deviations and power consumption, respectively, and $\mathbf{x}_{k_0}$ denote the initial condition. Finally, the feasible sets $\mathcal{U}$ and $\mathcal{X}$, define the constraints on the control input and state variables and are given by:

$$\mathcal{U} = \left\{ u_{i,j}(k) \in \mathbb{R}^+ \, \middle| \, 0 \le u_{i,j}(k) \le 0.4 \right\}, \qquad (23)$$

$$\mathcal{X} = \left\{ x_n(k) \in \mathbb{R}^+ \, \middle| \, x_{min_n} \le x_n(k) \le x_{max_n} \right\}. \qquad (24)$$

A. STABILITY OF THE CLOSED-LOOP SYSTEM
In this section, the stability arguments are provided for the proposed framework. This is achieved by employing the dynamics of the ACBN in Section II and constraints of the NLP in (21).

Consider the following Lyapunov functional:

$$V = e^T e + w_p P_T, \qquad (25)$$

where

$$e^T = [e_1 \quad e_2 \quad \dots \quad e_N].$$

The time derivative of V in (25) is given as:

$$\dot{V} = \dot{e}^T e + e^T \dot{e} + w_p \dot{P}_T$$

$$= 2 \left(e_1 \dot{e}_1 + \sum_{n=2}^{N-1} e_n \dot{e}_n + e_N \dot{e}_N \right) + w_p \dot{P}_T. \qquad (26)$$

Taking into account the SoC levels of any two adjacent cells, the NMPC operates the MOSFETs according to the corresponding charge levels. In an N-cell string connected in series, there are N^N possible combinations of how the initial charge level is distributed among the cells. However, stability can be proven by considering the two edge cases. In the first case, initial SoC among cells is distributed in the following manner: $x_1 > x_2 > \dots > x_N$, whereas the second case considers $x_1 < x_2 < \dots < x_N$. By considering (1) & (26), the stability of the closed-loop system is proved for both cases using the Lyapunov theory.

1) Stability Analysis for Case-1 ($x_1 > x_2 > \dots > x_N$):
In this case, during the charging phase, only the MOSFETs indexed $j = 1$, i.e., the odd combination of switches associated with each capacitor C_i will turn on to charge the C_i from the cell having higher SoC. Similarly, in the

discharging phase, MOSFETs indexed $j = 2$ will turn on, and consequently C_i will charge the cell with lower SoC.

Therefore, after considering that all the cells have the same capacity η, the expressions for $\dot{e}_1$, $\dot{e}_n$ and $\dot{e}_N$ can be derived as follows:

$$\dot{e}_1 = \frac{1}{N\eta} \left[(N-1)I_{1,1} - \Xi_1 - I_{(N-1),2} \right],$$

$$\dot{e}_n = \frac{1}{N\eta} \left[N \left(I_{n,1} + I_{(n-1),2} \right) - I_{1,1} - I_{(N-1),2} - \Xi_1 \right],$$

$$\dot{e}_N = \frac{1}{N\eta} \left[(N-1)I_{(N-1),2} - I_{1,1} - \Xi_1 \right], \qquad (27)$$

where $\Xi_1 = \sum_{n=2}^{N-1} \left(I_{n,1} + I_{(n-1),2} \right)$. Consequently, based on the selection of the parameters, as given in Section IV, and by assuming that the charging and discharging paths of the capacitor have the same resistance (R_i), the magnitudes of both $I_{i,1}$ and $I_{i,2}$ come out to be the same, and thus $|I_{i,1}| = |I_{i,2}| \le I^\star$. After using the results in (27), $\dot{e}_n = 0$ and $\Xi_1 = 0$ (same number of charging and discharging currents). For Case-I $e_1 > 0$ and $e_N < 0$, therefore, the time derivative of the Lyapunov functional in (26) becomes:

$$\dot{V} \le -\frac{2I^\star}{\eta} \left(|e_1| + |e_N| \right) + w_p \dot{P}_T. \qquad (28)$$

With the proper choice of w_p, it can then be ensured that $\dot{V} \le 0$, and subsequently, by using the invariant set theorem, it can be concluded that the SoC level of each cell converges to the average SoC level.

2) Stability Analysis for Case-2 ($x_1 < x_2 < \dots < x_N$):
In this case, during the charging phase, only the MOSFETs indexed $j = 2$, i.e., the even combination of switches associated with each capacitor C_i will turn on to charge the C_i from the cell having higher SoC. Similarly, in the discharging phase, MOSFETs indexed $j = 1$ will turn on, and consequently C_i will charge the cell with lower SoC. Similarly, the time derivatives of $\dot{e}_1$, $\dot{e}_n$ and $\dot{e}_N$ can be expressed as:

$$\dot{e}_1 = \frac{1}{N\eta} \left[(N-1)I_{1,2} - \Xi_2 - I_{(N-1),1} \right], \qquad (29)$$

$$\dot{e}_n = \frac{1}{N\eta} \left[N \left(I_{n-1,1} + I_{n,2} \right) - I_{1,2} - I_{(N-1),1} - \Xi_2 \right],$$

$$\dot{e}_N = \frac{1}{N\eta} \left[(N-1)I_{(N-1),1} - I_{1,2} - \Xi_2 \right],$$

where $\Xi_2 = \sum_{n=2}^{N-1} \left(I_{n,2} + I_{n-1,1} \right)$.

By taking into account the charging and discharging current's magnitude and the fact that $e_1 < 0$ and $e_N > 0$, similar results as of (28) can be obtained. By the same extension, the above argument can in turn be applied to prove the stability of the proposed framework for any initial SoC condition.

IV. RESULTS & DISCUSSIONS
The aim of the simulations is to evaluate the balancing performance of two distinct architectures—BB and SC—during overnight EV charging under the NMPC framework. Figure
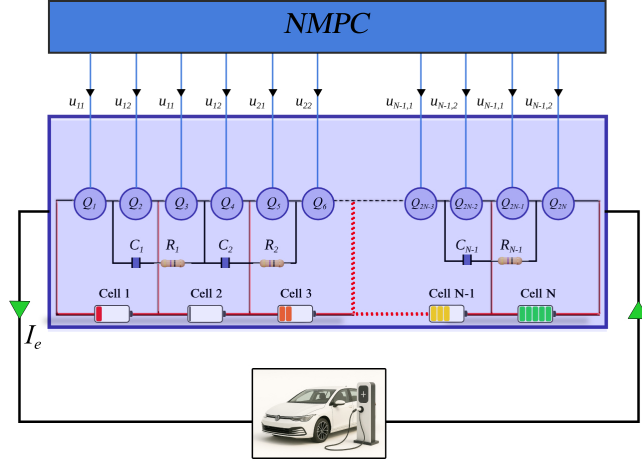
FIGURE 2: Control implementation scheme for NMPC-based ACB.

TABLE 1: Nominal model parameters for simulations

Parameter	Value	Parameter	Value
T	50 ms	t_d	$2\,\mu s$
η_{nom}	10800 As	R_{ds}	$5.3\,m\Omega$
t_f	8 ns	t_r	72 ns
R_C	$0.01\,\Omega$	C	$47\,\mu F$
R_0	$0.0441\,\Omega$		

2 demonstrates the control implementation scheme, wherein the NMPC, based on the knowledge of the current charge levels of all cells, generates duty cycles that are in turn utilized by MOSFETs of SC architecture to perform balancing. Moreover, the input current to the ACBN system is given by the charging station. The EV charging is usually divided into three levels: Level-1, Level-2 and Level-3, with each level having distinct voltage, current, and power rating specifications [34]. For instance, Level-1 charging uses standard 120V AC supply and typically delivers $12 - 16$ A, whereas Level-2 and Level-3 charging use 240V single-phase and 3-phase supply and deliver up to 60 A currents. Consequently, Level-1 is the most suitable for slow and overnight charging of EVs [35], and so is considered in this work as depicted in the schematic. Moreover, though a generalized framework comprising N cells is given in the figure, the simulations are performed for 3 cells. This is because in series-based adjacent cell-cell topology, a cell should be able to transfer charge to a maximum of two cells. Therefore, the lowest value of N that meets this condition is 3. In this configuration, the boundary cells (i.e., cells 1 and 3) can transfer charge to and from cell 2, while cell 2 can receive and give charge from both boundary cells, thereby capturing all the charge transfer paths.

The NMPC problem, as formulated in Section III, was solved in the MATLAB/CasADi environment employing the interior point optimizer algorithm (Ipopt). The value of T_p was set to 10 s, and the RK-45 method was used to discretize the dynamical system, as given in the (1), with a simulation step size of 10 s. Similarly, the electrical parameters of the 2.3 Ah A123 26650 LiFePO$_4$ cell as considered in the simulations are given in Table 1.

NMPC formulation allows for the incorporation of multiple conflicting objectives into its optimization problem, wherein the relative weights among objectives are left to the design engineer's discretion as deemed fit for the relevant problem. Therefore, in this work, extensive simulations were performed for both architectures by incrementally varying the weights of P_{loss} i.e., w_p in the NMPC cost function, and using Pareto analysis, a balance was found between balancing time (t_b) and P_{loss}. Similarly, t_b is set to be defined as a time instant when the standard deviation of SoC levels of all cells becomes 0.02, i.e., $\sigma(\vec{x}(k)) = 0.02$, and the simulations were performed until the SoC of any cell reaches the value of one, signifying the fully charged pack, and the initial state vector is $\begin{bmatrix} 0.1 & 0.2 & 0.3 \end{bmatrix}$. The remaining section will discuss the simulation results in the following structure: the local-level results of ACB for SC-based architecture will be given, which will be followed by a thorough comparison of performance metrics of BB- and SC-based ACB.

Figure 3 shows the SoC curve w.r.t. two different w_p: 0 and 0.015. Starting from the same initial values, the SoC curves corresponding to $wp = 0$ slowly converge to the balanced state in about 2.76 hours, whereas the curves for $wp = 0.015$ reaches the balanced state in about 6.36 hours. Moreover, it can also be seen from the figure that the pack takes less time to fully charge when the focus of the control problem is entirely on the balancing. Similarly, Figure 4 portrays the balancing currents corresponding to two different weights. It is obvious from the figure that when the focus is more tilted towards reducing power losses, the controller generates actions that result in lesser currents. However, at about the 5th hour, there is a sudden increase in the current values for cell 1. This is because by that time, cells 2 and 3 had achieved the balancing criterion, cell 1 was still far from the balanced state, and thus, in the cost function, only cell 1's balancing weights were dominant, momentarily causing the controller to take abrupt action. Moreover, Figure 5 shows the duty cycles generated by NMPC. For the second scenario, wherein both the conflicting objectives were activated, a continuous variation in control actions until the balancing criterion was achieved can be observed, unlike the first scenario of a single objective, where there is a smooth transition in the values of duty cycles. Similarly, Figure 6 compares the power losses for both scenarios. For case 1, it can be seen that power losses were high initially, and their value decreased with a decreasing rate. Moreover, in this case, though there was no focus on reducing losses, they still decreased; this is because as the cells approach the balanced state, the controller causes the lower value of balancing currents, ultimately resulting in decreasing power losses. Moreover, for the second case, the losses started at a relatively lower value. Though these losses remained higher than that of case 1, these values are marginal, resulting in the average losses of 6.6×10^{-3} and 4.5×10^{-3} W for case 1 and case 2, respectively.
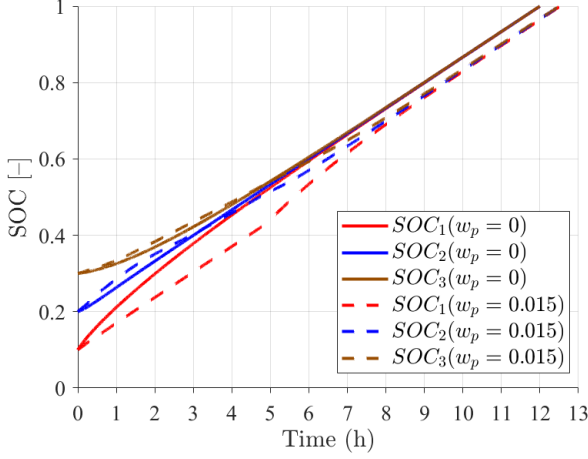
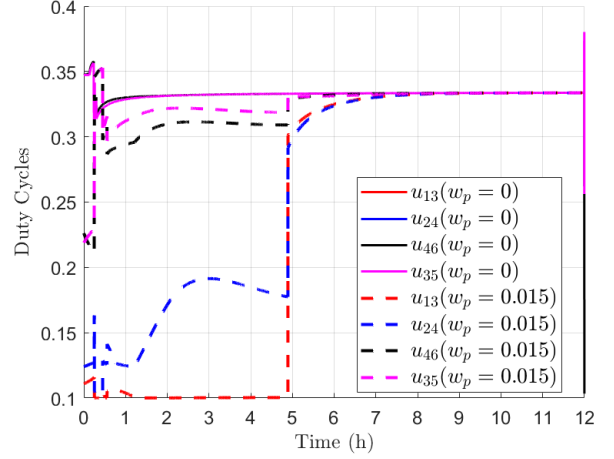FIGURE 3: SoC of SC architecture for different power losses weights

FIGURE 5: Control efforts of SC architecture for different weights
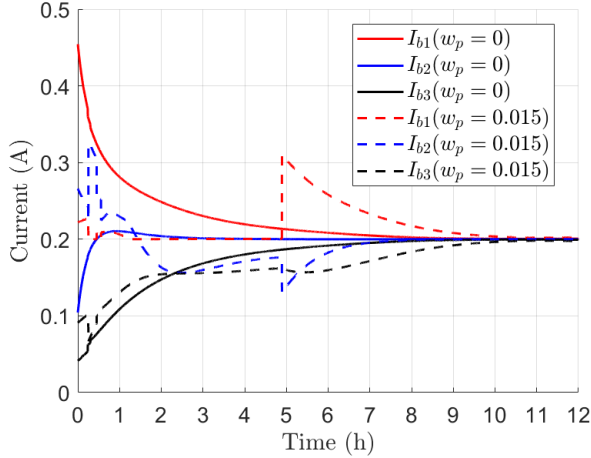

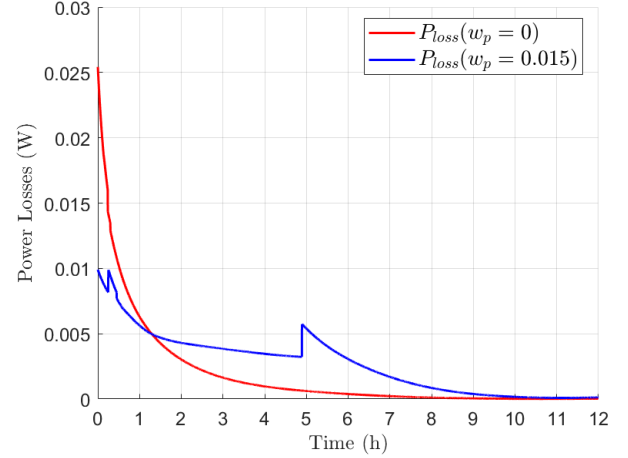FIGURE 4: Balancing currents of SC architecture for different weights

FIGURE 6: Power losses of SC architecture for different weights

Finally, the rest of the section is devoted to the main comparative analysis for ACB during overnight charging for the two architectures: SC and BB, where the model of BB is given in our earlier work [30]. Moreover, the following performance metrics are compared: balancing time (t_b), average power losses (P_{loss}), and energy dissipated (E_d), where E_d is defined as the integration of P_{loss} till the time instant when balancing occurs. As the range of these metrics lies in different regimes, they are properly normalized; for each metric, its value is divided by the maximum value attained by any architecture. Moreover, the NMPC simulations were performed by varying the weights of w_p of the NMPC's cost function (cf. (21)), and are given as follows: [0, 0.0005, 0.001, 0.003, 0.005, 0.007, 0.009, 0.01, 0.015]. 2 summarizes the performance comparison of the BB converter and SC architectures in terms of key matrices (balancing time, power losses, and energy dissipation) across

different weight conditions. Given this context of varying the values of w_p, a quick glance over Figures 7 and 8 reveals a fundamentally different trade-off pattern for both architectures. For the BB converter—cf. Figure 7, a loss-agnostic controller, i.e., $w_p = 0$ incurred the highest normalized value of P_{loss} as anticipated; whereas, in terms of balancing time, it equalized the cells quickly, yielding the normalized t_b value of 0.075. Moreover, as the penalty on P_{loss} was incrementally increased, its value dropped more than 60 % to the normalized value of 0.34 and E_d reached its minimum value by the time w_p became 0.003. Further increasing the values of w_p, resulted in a gradual drop in P_{loss}, however, E_d again started to increase, attaining its maximum value by the time $w_p = 0.15$; similarly, within this regime of w_p, the values of t_b saw a drastic increase, and it reached its highest value by $wp = 0.015$.

Overall, for BB, t_b increased monotonically as w_p in-

creased. Similarly, P_{loss} decreased rapidly at first till the time w_p reached its mid-values; however, beyond that, P_{loss} saw a gradual decrease. Finally, the E_d demonstrated non-monotonic behavior: followed by an initial decrease till $w_p = 0.003$, its values started increasing, almost tracing a U-shaped path.

On the contrary, the SC demonstrated a much more conservative behavior and stayed in the low-loss regime throughout the varying values of w_p. For instance, even for $w_p = 0$, the normalized t_b was 0.43 times more than that of BB, whereas the normalized P_{loss} was 0.12– 729 % lesser than that of BB converter's. Moreover, as the w_p increased, t_b and E_d growth were in positive correlation, wherein the normalized t_b attained the same value as BB's at $w_p = 0.015$, and normalized E_d reached its maximum value of 0.66—100% less than BB, whereas P_{loss} saw only a marginal decrease. This behavior stands in contrast to BB, which dynamically switches to a high balancing time/high losses and low balancing time/low losses mode. Overall, the SC architecture reveals more stable and predictable performance metrics in the face of varying w_p values, and the trade-offs are more discernible than those of BB's. This is further delineated by Figure 9: it can clearly be seen that these performance metrics are conflicting in nature, and not all of them can simultaneously be optimized; thus, a compromise has to be reached by iteratively changing the weights. However, to select a single value of w_p that finds a perfect balance between these three performance metrics for each architecture, a knee point was found for the data, as depicted in Figure 9, using the minimum distance approach [36]. This works by finding a weight whose distance is minimum from the hypothetically ideal scenario, i.e., where all metrics have the lowest value—usually taken as the origin point. Consequently, for SC architecture, w_p was found to be 0.001, and similarly, for BB, w_p came out to be 0.003. The corresponding performance metrics for these weights can be seen in Table 2.

These results, as discussed above, clearly demonstrate that when balancing speed is not the immediate objective, then SC-based architecture is a preferable choice, as it can yield losses that are 729 % less than losses incurred by the BB converter. This is because in each charging cycle, SC incurs losses due to MOSFET's conduction and switching losses; on the contrary, for the same charging cycle, BB accumulates charges due to inductor, switching, and diode losses. Moreover, in BB, the inductor currents can become higher, which leads to higher balancing current, resulting in lower balancing time, whereas in SC, the balancing current's magnitude is constrained by the capacitance of the capacitor, which, once deployed, remains fixed. This selection is suitable for an overnight EV charging scenario, where time is not the constraint and the focus is on cutting down on energy losses.

V. CONCLUSIONS

Cell balancing is an integral aspect of any battery management system for the better performance and health of a bat-
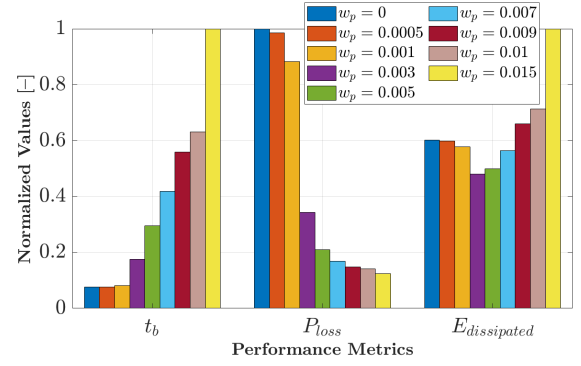

FIGURE 7: Bar graph of BB architecture for performance metrics
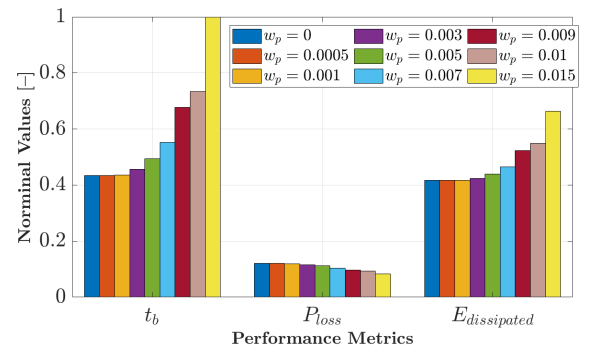

FIGURE 8: Bar graph of SC architecture for performance metrics
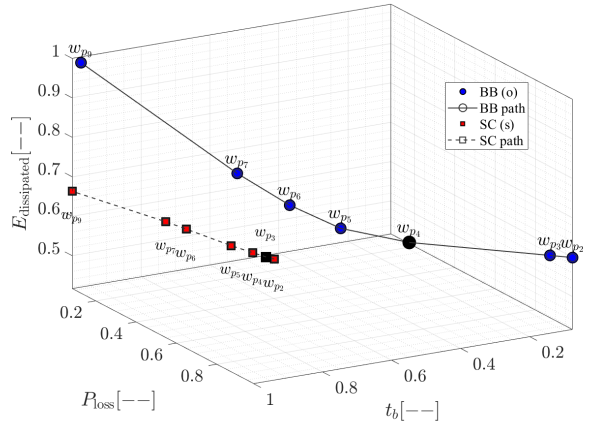

FIGURE 9: Pareto graph of both SC & BB Architectures

tery pack. However, variations, i.e., selection of power electronic components in active cell balancing architecture, result in different performance metrics: balancing time, power losses, energy dissipation, etc. Therefore, in this work, active cell balancing is performed by deriving high-fidelity balancing currents and power losses for SC-based architecture for a N serially connected adjacent cell-to-cell battery pack. The balancing was performed under an NMPC framework,

TABLE 2: Performance comparison in terms of balancing time, power losses, and energy dissipation for varying NMPC weights

Sr. No	Weight w_p	t_b [s] (BB)	t_b [s] (SC)	P_{loss} [W] (BB)	P_{loss} [W] (SC)	E_d [J] (BB)	E_d [J] (SC)
1	0	1725	9935	0.0547	0.0066	94.147	65.258
2	0.0005	1740	9950	0.0539	0.0066	93.608	65.214
3	0.001	1870	9960	0.0483	0.0065	90.322	65.161
4	0.003	4005	10465	0.0188	0.0063	75.064	66.366
5	0.005	6775	11300	0.0115	0.0061	77.881	68.756
6	0.007	9595	12640	0.0092	0.0057	88.169	72.597
7	0.009	12810	15505	0.0081	0.0053	103.193	81.730
8	0.010	14440	16810	0.0077	0.0051	111.354	85.813
9	0.015	22865	22895	0.0068	0.0045	156.286	103.642

and extensive simulations were performed to compare the performance of SC with BB converter under the same settings. The results demonstrated that balancing under SC-based architecture can incur up to 288 % fewer losses than balancing under BB converter, making the former a suitable choice for overnight EV charging.

As the thermal properties of a cell play an important role in the balancing performance, the future work involves integrating the electro-thermal model into the current framework and other balancing topologies, such as layer- and module-based topologies.

REFERENCES

[1] A. Aghmadi and O. A. Mohammed, "Energy storage systems: Technologies and high-power applications," Batteries, vol. 10, no. 4, 2024. [Online]. Available: https://www.mdpi.com/2313-0105/10/4/141

[2] L. Wang, Y. Fang, L. Wang, F. Yun, J. Wang, and S. Lu, "Understanding discharge voltage inconsistency in lithium-ion cells via statistical characteristics and numerical analysis," IEEE Access, vol. 8, pp. 84 821–84 836, 2020.

[3] M. Uzair, G. Abbas, and S. Hosain, "Characteristics of battery management systems of electric vehicles with consideration of the active and passive cell balancing process," World Electric Vehicle Journal, vol. 12, no. 3, 2021. [Online]. Available: https://www.mdpi.com/2032-6653/12/3/120

[4] N. Khan, C. A. Ooi, A. Alturki, M. Amir, Shreasth, and T. Alharbi, "A critical review of battery cell balancing techniques, optimal design, converter topologies, and performance evaluation for optimizing storage system in electric vehicles," Energy Reports, vol. 11, pp. 4999–5032, 2024. [Online]. Available: https://www.sciencedirect.com/science/article/pii/S2352484724002506

[5] A. Habib, M. Hasan, G. Issa, D. Singh, S. Islam, and T. Ghazal, "Lithium-ion battery management system for electric vehicles: Constraints, challenges, and recommendations," Batteries, vol. 9, no. 3, p. 152, 2023. [Online]. Available: https://www.mdpi.com/2313-0105/9/3/152

[6] J. Chen, Z. Zhou, Z. Zhou, X. Wang, and B. Liaw, "Impact of battery cell imbalance on electric vehicle range⋆," Green Energy and Intelligent Transportation, vol. 1, no. 3, 2022. [Online]. Available: https://www.sciopen.com/article/10.1016/j.geits.2022.100025

[7] Y. A. Sultan, A. A. Eladl, M. A. Hassan, and S. A. Gamel, "Enhancing electric vehicle battery lifespan: integrating active balancing and machine learning for precise rul estimation," Scientific Reports, vol. 15, no. 1, Jan 2025.

[8] R. Azam, A. Ahmed, A. Arshad, and Q. Ahmed, "Nonlinear model predictive control design for active cell balancing and thermal management," 08 2024, pp. 46–51.

[9] T. Hein, A. Ziegler, D. Oeser, and A. Ackva, "A capacity-based equalization method for aged lithium-ion batteries in electric vehicles," Electric Power Systems Research, vol. 191, p. 106898, 2021. [Online]. Available: https://www.sciencedirect.com/science/article/pii/S0378779620306969

[10] M.-C. Dinh, T.-T. Le, and M. Park, "A low-cost and high-efficiency active cell-balancing circuit for the reuse of ev batteries," Batteries, vol. 10, no. 2, 2024. [Online]. Available: https://www.mdpi.com/2313-0105/10/2/61

[11] G. Noh, J. Lee, and J.-I. Ha, "Design and analysis of single-inductor power converter for both battery balancing and voltage regulation," IEEE Transactions on Industrial Electronics, vol. 69, no. 3, pp. 2874–2884, 2022.

[12] Y. Ye, J. Lin, Z. Li, and X. Wang, "Double-tiered cell balancing system with switched-capacitor and switched-inductor," IEEE Access, vol. 7, pp. 183 356–183 364, 2019.

[13] K. Liu, Z. Yang, X. Tang, and W. Cao, "Automotive battery equalizers based on joint switched-capacitor and buck-boost converters," IEEE Transactions on Vehicular Technology, vol. 69, no. 11, pp. 12 716–12 724, 2020.

[14] T. Conway, "An isolated active balancing and monitoring system for lithium ion battery stacks utilizing a single transformer per cell," IEEE Transactions on Power Electronics, vol. 36, no. 4, pp. 3727–3734, 2021.

[15] C. N. Van, "Optimal control of active cell balancing for lithium-ion battery pack with constraints on cells' current and temperature," Journal of Electrochemical Energy Conversion and Storage, vol. 20, no. 1, p. 011009, 05 2022. [Online]. Available: https://doi.org/10.1115/1.4054530

[16] P. Kremer, F. Cigarini, D. Göhlich, and S. Park, "Active cell balancing for life cycle extension of lithium-ion batteries under thermal gradient," in 2021 IEEE/ACM International Symposium on Low Power Electronics and Design (ISLPED), 2021, pp. 1–6.

[17] Z. Xia and J. A. Abu Qahouq, "State-of-charge balancing of lithium-ion batteries with state-of-health awareness capability," IEEE Transactions on Industry Applications, vol. 57, no. 1, pp. 673–684, 2021.

[18] A. Pröbstl, S. Park, S. Narayanaswamy, S. Steinhorst, and S. Chakraborty, "Soh-aware active cell balancing strategy for high power battery packs," in 2018 Design, Automation & Test in Europe Conference & Exhibition (DATE), 2018, pp. 431–436.

[19] F. S. J. Hoekstra, H. J. Bergveld, and M. C. F. Donkers, "Optimal control of active cell balancing: Extending the range and useful lifetime of a battery pack," IEEE Transactions on Control Systems Technology, vol. 30, no. 6, pp. 2759–2766, 2022.

[20] J. Chen, A. Behal, Z. Li, and C. Li, "Active battery cell balancing by real-time model predictive control for extending electric vehicle driving range," IEEE Transactions on Automation Science and Engineering, vol. 21, no. 3, pp. 4003–4015, 2024.

[21] Y. Liu, C. Xia, M. Gu, W. Xin, and X. Men, "A novel active equalizer for li-ion battery pack in electric vehicles," Energy Procedia, vol. 158, pp. 2649–2654, 2019, innovative Solutions for Energy Transitions. [Online]. Available: https://www.sciencedirect.com/science/article/pii/S1876610219310951

[22] H. Ren, Y. Zhao, S. Chen, and T. Wang, "Design and implementation of a battery management system with active charge balance based on the soc and soh online estimation," Energy, vol. 166, pp. 908–917, 2019. [Online]. Available: https://www.sciencedirect.com/science/article/pii/S0360544218321297

[23] S.-L. Wu, H.-C. Chen, and C.-H. Chien, "A novel active cell balancing circuit and charging strategy in lithium battery pack," Energies, vol. 12, no. 23, 2019. [Online]. Available: https://www.mdpi.com/1996-1073/12/23/4473

[24] L. Song, T. Liang, L. Lu, and M. Ouyang, "Lithium-ion battery pack equalization based on charging voltage curves," International Journal of Electrical Power & Energy Systems, vol. 115, p. 105516, 2020. [Online]. Available: https://www.sciencedirect.com/science/article/pii/S0142061519302364

[25] S. Singirikonda and Y. Obulesu, "Active cell voltage balancing of electric vehicle batteries by using an optimized switched capacitor strategy," Journal of Energy Storage, vol. 38, p. 102521, 2021. [Online]. Available: https://www.sciencedirect.com/science/article/pii/S2352152X21002693

[26] Z. Zhang, L. Zhang, L. Hu, and C. Huang, "Active cell balancing of lithium-ion battery pack based on average state of charge," International Journal of Energy Research, vol. 44, no. 4, pp. 2535–2548, 2020. [Online]. Available: https://onlinelibrary.wiley.com/doi/abs/10.1002/er.4876

[27] F. Zhou, H. Lin, J. Hu, Z. Lv, B. Qian, and J. Xu, "A novel balancing strategy for series-connected lithium batteries based on mixed charging mode," in 2014 International Power Electronics and Application Conference and Exposition, 2014, pp. 732–736.

[28] D. Thiruvonasundari and K. Deepa, "Optimized passive cell balancing for fast charging in electric vehicle," IETE Journal of Research, vol. 69, no. 4, pp. 2089–2097, 2023. [Online]. Available: https://doi.org/10.1080/03772063.2021.1886604

[29] S. B. Javed, A. A. Uppal, M. R. Azam, K. Shehzad, and Q. Ahmed, "Model-based quantitative analysis of a capacitive cell balancing technique using soc estimator," in 2022 IEEE Conference on Control Technology and Applications (CCTA), 2022, pp. 670–675.

[30] S. Bilal Javed, A. A. Uppal, M. R. Azam, and Q. Ahmed, "Model-based quantitative analysis of power losses-aware active cell balancing networks with load," IEEE Transactions on Transportation Electrification, vol. 11, no. 1, pp. 4179–4188, 2025.

[31] A. Arshad, S. Javed, and Q. Ahmed, "Power losses aware nonlinear model predictive control design for active cell balancing," IEEE Control Systems Letters, vol. PP, pp. 3705–3710, 12 2023.

[32] A. Ahmed, A. Arshad, Q. Ahmed, and R. Azam, "Performance analysis of model predictive controllers for active cell balancing of electric vehicle battery," 08 2024, pp. 288–293.

[33] P. Kollmeyer, C. Vidal, M. Naguib, and M. Skells, "LG 18650HG2 Li-ion Battery Data and Example Deep Neural Network xEV SOC Estimator Script," Mendeley Data, 2020. [Online]. Available: https://data.mendeley.com/datasets/cp3473x7xv/3

[34] L. Bao, L. Fan, and Z. Miao, "Real-time simulation of level 1, level 2, and level 3 electric vehicle charging systems," 2021. [Online]. Available: https://arxiv.org/abs/2111.02506

[35] K. Knowles, B. Faye, A. Orrson, H. Abdeltawab, M. Bayrakci-Boz, and S. Anwar, "Optimal ev charger level specification for residential buildings with renewable energy," in IEEE EUROCON 2021 - 19th International Conference on Smart Technologies, 2021, pp. 426–431.

[36] S. Khoshnevisan, W. Gong, L. Wang, and C. H. Juang, "Robust design in geotechnical engineering – an update," Georisk: Assessment and Management of Risk for Engineered Systems and Geohazards, vol. 8, no. 4, pp. 217–234, 2014. [Online]. Available: https://doi.org/10.1080/17499518.2014.980274

AFAQ AHMED received his B.Eng. and M.S. degrees in Electrical Engineering from Ghulam Ishaq Khan Institute and COMSATS University Islamabad, Pakistan, in 2015 and 2023, respectively. He is currently serving as a research assistant at COMSATS University Islamabad. His research interests include mathematical modeling and simulation of battery management systems, development of balancing architectures, and applications of learning-based predictive control.

DR. ALI ARSHAD UPPAL received his PhD degree in Electrical Engineering (Control Systems) from COMSATS University Islamabad (CUI), Islamabad, Pakistan in 2016. During his Ph.D., from 2015—2016, he worked as a visiting scholar at the Department of Electrical and Computer Engineering, The Ohio State University, Columbus, OH, USA. From 2020—2021, he worked as a postdoctoral researcher at the Faculty of Engineering, University of Porto, Porto, Portugal. He is currently working as a Tenured Associate Professor at the Department of Electrical Engineering, CUI. He has been elected to the grade of Senior Member, IEEE in recognition of his research contributions in the field of Control Systems in June 2022. His research interests include application of nonlinear control in the areas of energy conversion, energy storage and clean energy technologies. He is currently working on the modelling and control of active cell balancing of Lithium-ion batteries to extend the range of electric vehicles. So far, he has secured competitive research funding of worth around 20 million PKR; and authored/co-authored several research papers in peer-reviewed journals and international conferences. Moreover, he has managed a special issue: Sliding Mode Control in Dynamic Systems, MDPI Electronics, as a guest editor.

MUHAMMAD AZMAT ULLAH completed his B.S. in Electronic Engineering from the International Islamic University Islamabad, Pakistan, in 2012, and obtained his M.S. degree in Electrical Engineering from Government College University Lahore in 2015. He is currently pursuing a Ph.D. in Electrical Engineering with a specialization in Control Systems at COMSATS University Islamabad, Pakistan. His research interests include nonlinear control systems, model predictive control, and battery management systems. He is currently working on MPC-based active cell balancing for lithium-ion battery networks.

QADEER AHMED is an Assistant Professor and director of Mobility Systems Lab (MSL) at the Department of Mechanical and Aerospace Engineering at The Ohio State University and a fellow of OSU's Center for Automotive Research. His research focus is connected, automated, safe, and energy-efficient vehicular/mobility systems. He has authored more than 127 international peer-reviewed publications. He has also served as Editor for IFAC Advances in Automotive Control 2022 and is associate editor of IEEE Transactions on Transportation Electrification and IEEE/ASME Transactions on Mechatronics. He is a recipient of SAE's Ralph R. Teetor Educational Award in 2023, SAE's L. Ray Buckendale Award in 2019, and OSU's Lumley Research Award in 2018.

• • •